PCCP

Accepted Manuscript

This is an *Accepted Manuscript*, which has been through the Royal Society of Chemistry peer review process and has been accepted for publication.

Accepted Manuscripts are published online shortly after acceptance, before technical editing, formatting and proof reading. Using this free service, authors can make their results available to the community, in citable form, before we publish the edited article. We will replace this *Accepted Manuscript* with the edited and formatted *Advance Article* as soon as it is available.

You can find more information about *Accepted Manuscripts* in the Information for Authors.

Please note that technical editing may introduce minor changes to the text and/or graphics, which may alter content. The journal's standard Terms & Conditions and the Ethical guidelines still apply. In no event shall the Royal Society of Chemistry be held responsible for any errors or omissions in this *Accepted Manuscript* or any consequences arising from the use of any information it contains.

ROYAL SOCIETY OF CHEMISTRY

www.rsc.org/pccp

Journal Name

RSCPublishing

ARTICLE

Magnetic γ-Fe_2O_3, Fe_3O_4, and Fe nanoparticles confined within ordered mesoporous carbons as efficient microwave absorbers

Cite this: DOI: 10.1039/x0xx00000x

Received 00th January 2012,
Accepted 00th January 2012

DOI: 10.1039/x0xx00000x

www.rsc.org/

Jiacheng Wang,*[a] Hu Zhou,[a,b] Jiandong Zhuang[a] and Qian Liu*[a]

A series of magnetic γ-Fe_2O_3, Fe_3O_4, and Fe nanoparticles have been successfully introduced into the mesochannels of ordered mesoporous carbons by the combination of the impregnation of iron salt precursors and then *in situ* hydrolysis, pyrolysis and reduction processes. The magnetic nanoparticles are uniformly dispersed and confined within the mesopores of mesoporous carbons. Although the as-prepared magnetic mesoporous carbon composites have high contents of magnetic components, they still possess very high specific surface areas and pore volumes. The magnetic hysteresis loops measurements imply that the magnetic constituents are poorly-crystalline nanoparticles and their saturation magnetization is evidently smaller than bulky magnetic materials. The confinement of magnetic nanoparticles within the mesopores of mesoporous carbons results in the decrease of the complex permittivity and the increase of the complex permeability of the magnetic nanocomposites. The maximum reflection loss (RL) values of -32 dB at 11.3 GHz and a broad absorption band (over 2 GHz) with RL values < -10 dB are obtained for 10-Fe_3O_4/CMK-3 and 10-γ-Fe_2O_3/CMK-3 composite in a frequency range of 8.2-12.4 GHz (*X*-band), showing their great potentials in microwave absorption. This research opens a new method and idea for developing novel magnetic mesoporous carbon composites as high-performance microwave absorbing materials.

1. Introduction

Recently, serious electromagnetic interference (EMI) pollution continuously receives great attention because of explosive development of electrical and electronic industries. The strong EMI pollution not only can lead to disturbances on various systems and equipment for civil and military applications, but also is potentially harmful to human health. Thus, many efforts have been focused on exploiting effective microwave absorption and shielding materials with low density and strong absorption in a wide frequency range to attenuate those unneeded electromagnetic (EM) energies.[1] Compared with metal-based EMI shielding and absorbing materials, carbon-based conducting composites are becoming attractive because of their light weight, high chemical stability, low cost, and excellent adaptability to a wider range of environments.[2] Various nanostructured carbon-based materials have been studied not only in many applications including heterogeneous catalysis,[3] electrocatalysis,[4] gas adsorption/storage,[5] energy storage,[5c, 6] and other areas,[7] but also as EM shielding and absorbing materials, especially in the case of harsh working environments. These studies on carbonaceous EM wave shielding and absorbing materials are related to carbon black (CB),[8] carbon nanofibers (CNFs),[9] carbon nanotubes (CNTs),[8a, 10] carbon foams,[11] and graphene,[12] *etc*.

Among these nanosized carbons, ordered mesoporous carbons, prepared by the hard template *via* nanocasting ordered mesoporous silicas[13] or the soft template *via* self-assembly of polymer precursors and organic surfactants,[14] possess high specific surface areas and special mesostructure of ordered nanowire/nanopore arrays. Specially, CMK-3, a kind of ordered mesoporous carbon templated from ordered mesopore silica SBA-15, is of particular interest due to its fascinating properties, such as large surface area, unique electric behaviour, and highly ordered nanowire arrays interconnected by short carbon rods.[15] We have found that ordered mesoporous carbons are excellent candidates as EM wave shielding and absorbing fillers. A novel type of CMK-3/fused silica ceramic composite was successfully prepared by embedding CMK-3 particles within the silica matrix. The as-formed composite demonstrated a high RL value of more than -30 dB.[16] The spatial configurations of ordered mesoporous carbons have great influences on the EMI shielding efficiency (SE) of ordered mesoporous carbon/silica composites, and the EMI SE of the composites in the *X*-band frequency range decreased for the carbon mesostructures in the following order: CMK-3-filled > CMK-1-filled > CS41-filled.[17] As a microwave absorber, ordered mesoporous carbon is characteristic by large dielectric loss, light weight, and low cost. However, the dielectric permittivity and magnetic permeability of pure mesoporous carbon are out of balance. Thus, most of microwave radiation is

Physical Chemistry Chemical Physics Accepted Manuscript

reflected, rather than absorbed by pure carbon. In previous research, we prepared CMK-3-filled poly(methyl methacrylate) (PMMA) composites by *in-situ* polymerization and grafting of methyl methacrylate (MMA) on the surface of CMK-3 particles.[18] The microwave absorbing ability was evidently enhanced compared to the composite prepared by the solvent mixing method[19] due to the improved microwave impedance matching by adjusting the complex dielectric permittivity and further improving the dielectric loss of the *in situ* polymerized composite.[18] Alternatively, various magnetic species can be composited with porous carbons to increase the magnetic loss ability of the carbon composites.[20] The magnetic particles play important roles in improving the complex permeability owing to their large saturation magnetization.[21] Thus the microwave absorbing ability of the magnetic carbon composites can be increased because the impedance matching requirement is achieved. It has been reported that the magnetic CNTs composites formed by encapsulating magnetic particles within the channels of CNTs or absorbing magnetic particles on the surface of CNTs demonstrated the enhanced ability of microwave absorbance within a wide frequency range.[22] However the low surface areas of CNTs resulted in the formation of larger magnetic particles supported on CNTs, thus evidently decreased the microwave absorbing ability. And due to their large length-to-diameter ratios, CNTs tend to tangle together and it is difficult to disperse CNTs into various solutions homogeneously without any aggregation. Because of excellent textures (very high specific surface areas and short length-to-diameter ratios) of CMK-3 particles, magnetic nanoparticles can be introduced within the mesopores of ordered mesoporous carbon CMK-3 to form magnetic mesoporous carbon composites as high-performance microwave absorbers.

Generally, small amount of metal precursors could be effectively encapsulated within the mesopores of CMK-3 by impregnation and further be transformed to poorly crystallized nanoparticles under the low-temperature heat-treatment.[23] However, the resultant nanoparticles could aggregate strongly to form big particles on the carbon surface when very high content of metal precursors existed in CMK-3 mesopores or the transformation temperature increased.[24] Thus it is difficult to load high content (> 20 wt%) of homogeneously dispersed, non-aggregated, and crystalline nanoparticles within the mesopores. For example, due to the low melting point (47 °C) and boiling point (125 °C) of ferric nitrate, ($Fe(NO_3)_3$), it easily melts and aggregates into bigger particles outside the mesopores of mesoporous carbon upon the heat-treatment before it decomposes when mesoporous carbon is filled with high contents of $Fe(NO_3)_3$. Finally the as-formed product is heterogeneous mixture composed of magnetic particles and mesoporous carbon. The key to solve this problem is to efficiently control the diffusion/decomposition/aggregation process of high content of metal nitrate precursors in the mesopores during the pyrolysis process.

In this paper, we adopt a simple, controllable process to prepare magnetic ordered mesoporous carbon nanocomposites by a combined process of impregnation, pre-hydrolysis, and reduction. The iron salt introduced into the mesopores is *in situ* hydrolyzed in an ammonia atmosphere to produce iron hydroxide in the mesopores of ordered mesoporous carbon. Followed by a reduction process, different magnetic γ-Fe_2O_3, Fe_3O_4, and Fe nanoparticles confined within ordered mesoporous carbons were formed, in which the magnetic nanoparticles have high contents of up to 40 wt% and they are homogeneously confined within the mesopores. The structural textures of mesoporous carbons filled with designed magnetic nanoparticles have been characterized in detail. The microwave absorption properties of the magnetic nanocomposites were also investigated in a frequency range of *X*-band widely used in military and commercial fields. The confinement of magnetic species within ordered mesoporous carbons contributes to a better impedance matching, which results in the microwave absorption enhancement in the *X*-band.

2. Experimental

2.1 Reagents

Ordered mesoporous silica SBA-15 powders were purchased from Fudan University, China. Sucrose, ferric nitrate ($Fe(NO_3)_3$), hydrofluoric acid, sulfuric acid and anhydrous ethanol were purchased from Sinopharm Chemical Reagent Co., Ltd. All chemicals were used as received without any further purification. Deionized water was used in all experiments.

2.2 Materials synthesis

Ordered mesoporous carbon CMK-3 was synthesized by using SBA-15 as hard template according to the previously reported literature.[13b] The magnetic ordered mesoporous carbon nanocomposite precursor was prepared by an impregnation method followed by in situ hydrolysis, calcination, and reduction, as schematically shown in Fig. 1.[25] Typically, CMK-3 (1.2 g) was added to 20 mL of $Fe(NO_3)_3$ (4 or 10 mmol) ethanol solution. The suspension was vigorously stirred at room temperature until the solvent was completely evaporated to obtain dry powder. Then this powder was poured into a high glass bottle which stood in a beaker containing 10 mL of aqueous ammonia solution (concentration: 14 wt%) to avoid direct contact of the powder and solution. After the beaker was sealed, it was heated in a drying oven at 60 °C for 3 h to *in situ* hydrolyze $Fe(NO_3)_3$ in the mesopores of CMK-3. Then, the hydrolyzed product was washed with a small amount of water and ethanol, and calcinated in air at 200 °C for 2 h to obtain α-Fe_2O_3-filled CMK-3 (α-Fe_2O_3/CMK-3). The resultant α-Fe_2O_3/CMK-3 powder, equally divided into three parts, was further thermally treated to form magnetic Fe-containing CMK-3 nanocomposites. Reduction of α-Fe_2O_3/CMK-3 at 320 and 400 °C for 6 h in an Ar/H_2 atmosphere (5% H_2) led to the formation Fe_3O_4/CMK-3 and Fe/CMK-3 composite, respectively. The as-prepared Fe_3O_4/CMK-3 composite was heated at 150 °C for 2 h in air to form γ-Fe_2O_3/CMK-3 nanocomposite. The resulting magnetic Fe-containing CMK-3 composites are denoted as *x*-Fe_3O_4/CMK-3, *x*-Fe/CMK-3, and *x*-γ-Fe_2O_3/CMK-3, where *x* represents the content (mmol) of $Fe(NO_3)_3$ added initially.

2.3 Materials characterization

Physical Chemistry Chemical Physics Accepted Manuscript

This journal is © The Royal Society of Chemistry 2012

The as-synthesized composite powders were characterized by X-ray diffraction (XRD) on a D/MAX-RB X-ray diffractometer (Rigaku, Japan) using Cu-Kα_1 (λ=0.15406 nm) radiation at 40 KV and 60 mA. The morphology and mesopore structure were observed by scanning electron microscopy (SEM) (JSM-6700F JEOL, 10.0KV) equipped with EDS elemental analysis, and transmission electron microscopy (TEM) (JEM-2100F JEOL, 200KV). Thermogravimetric (TG) was carried out using a thermal analysis system (STA 449/C, Netzsch) with the samples heated in flowing air at a ramp of 10 ^{o}C/min. The nitrogen adsorption measurements were performed at -196 °C to investigate the pore structure of pristine CMK-3 and Fe-containing CMK-3 using Micromeritics ASAP2010 System (Micromeritics, Norcross, GA). Specific surface areas were calculated using the Brunauer-Emmett-Teller (BET) equation (p/p_0 = 0.05-0.2).[26] The total pore volume was determined at relative pressure p/p_0 = 0.99. The pore size distribution was estimated by the Barrett-Joyner-Halenda (BJH) method. The magnetic hysteresis loop was recorded on a Quantum Design PPMS system at 30 ^{o}C. For the measurements of microwave absorption properties by using waveguide technique, the magnetic powders were dispersed in commercial epoxy resin, which is generally used as binder matrix. In the mixture of magnetic Fe-containing CMK-3-resin, the weight percent of the magnetic powders was controlled to be 20 wt%. Then the mixture was pressed into a mold with a size of 22.86 mm (length) × 10.16 mm (width) to fit the waveguide sample holder in the network analyzer. The complex permittivity and permeability was measured by using a vector network analyzer (8722ES, HP) in the *X*-band. The microwave absorbing properties were deduced by calculating based on the transmission line theory related to the permittivity and permeability measured experimentally.

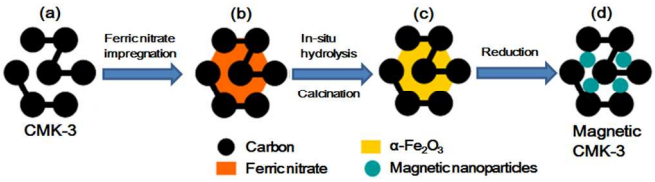

Fig. 1 Schematic drawing showing the synthesis of ordered mesoporous carbon CMK-3 filled with magnetic nanoparticles. (a) Ordered mesoporous carbon CMK-3 prepared using SBA-15 silica as hard template; (b) CMK-3/ferric nitrate precursor synthesized by an impregnation procedure; (c) *In situ* hydrolysis and calcination of CMK-3/ferric nitrate to form α-Fe_2O_3/CMK-3 composite. (d) The reduced magnetic CMK-3 by thermally treating CMK-3/α-Fe_2O_3 in flowing 5% H_2/Ar.

3. Results and Discussion

CMK-3 carbon, prepared by nanocasting SBA-15 silica with carbon, is composed of aggregated rod-like particles in sub-micrometer size, similar to its parent template.[15b, 27] After *in situ* filling the mesopores of CMK-3 with α-Fe_2O_3, SEM images of α-Fe_2O_3/CMK-3 composite confirms that it still consists of bundles of oriented arranged short carbon rods, forming mesoporous carbon particles with about 5 μm in diameter (Fig. 2b). As a result of *in situ* hydrolysis process, there is no aggregation of large Fe_2O_3 particles observed outside CMK-3 carbon particles (Fig. 2a-b), although the α-Fe_2O_3 content is as high as 40 wt% in 10-α-Fe_2O_3/CMK-3 composite. Moreover, high-resolution TEM image of the α-Fe_2O_3/CMK-3 composite shows both the maintenance of highly ordered mesoporous channels of CMK-3 carbon and high dispersion of small dark clusters that correspond to α-Fe_2O_3 nanoparticles (Fig. 2c). Due to the confinement effect of the mesoporous channels of CMK-3, the α-Fe_2O_3 nanoparticles are incorporated within ordered mesochannels and thus look like narrow. The estimated sizes of these particles are 5-9 nm in diameter and 10-40 nm in length. The corresponding EDS elemental analysis also indicates that the main elements are C, O and Fe in 10-α-Fe_2O_3/CMK-3 (Fig. 2d). The total contents of Fe and O in this composite are 41.4 wt% based on EDS analysis, which matches well with the theoretical content (40 wt%) of α-Fe_2O_3 in 10-α-Fe_2O_3/CMK-3. All these results indicate that the magnetic precursor (α-Fe_2O_3) was retained in the ordered mesopores of CMK-3 and a homogeneous α-Fe_2O_3/CMK-3 nanocomposite powder was formed by an impregnation method in combination with *in situ* hydrolysis and calcination procedure.

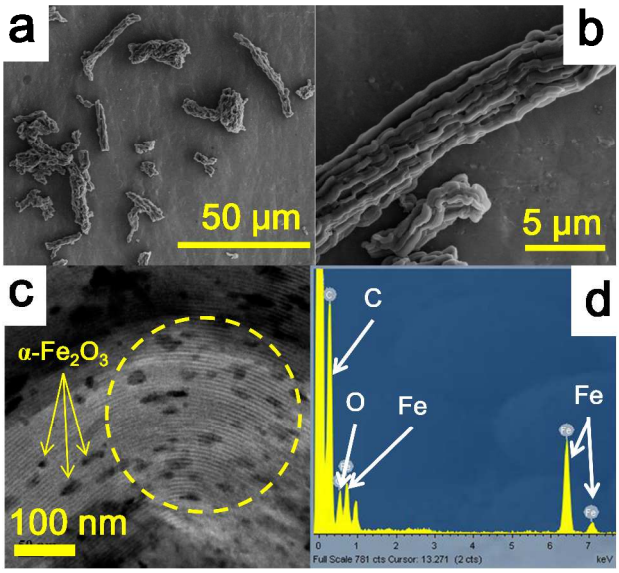

Fig. 2 (a, b) SEM and (c) TEM micrographs of 10-α-Fe_2O_3/CMK-3, and (d) EDS elemental analysis on the yellow circle area marked in the image of Fig. 2c.

The non-magnetic α-Fe_2O_3 in CMK-3 was further reduced in 5% H_2/Ar to form magnetic CMK-3 nanocomposite. The temperature is a very important parameter to affect the transformation of α-Fe_2O_3 to Fe_3O_4.[28] The optimum reduction temperature varied within 300-400 °C depending on different surrounding environments of α-Fe_2O_3.[29] Fig. S1 in the Electronic Supporting Information (ESI) shows the XRD patterns of 10-α-Fe_2O_3/CMK-3 composite reduced in 5% H_2/Ar at different temperatures (280, 320, or 350 °C) for 6 h. The XRD pattern of 10-α-Fe_2O_3/CMK-3 reduced at 320 °C presents several resolved diffraction peaks (Fig. 3 and S1), all of which are assigned to magnetite Fe_3O_4 (JCPDS card 19-0629). The

Physical Chemistry Chemical Physics Accepted Manuscript

lower reduction temperature (280 °C) resulted in the incomplete reduction of α-Fe_2O_3 and the higher temperature (350 °C) led to the formation of zero-valent Fe nanoparticles in final product (Fig. S1). Thus, the optimal temperature for the transformation of α-Fe_2O_3 to Fe_3O_4 within the mesopore of CMK-3 carbon is 320 °C. During the reduction process, α-Fe_2O_3 in the mesopores of CMK-3 is converted to magnetite and endows CMK-3 carbon particles with a magnetic property.

The further increase in the reduction temperature to 400 °C promoted the complete transformation of α-Fe_2O_3 to magnetic Fe metal in the mesopore of CMK-3, as confirmed by the XRD analysis (Fig. 3). The sharp reflections can be attributed to the body-centered cubic phase of Fe (JCPDS card 06-0696), without indication of the precursor or other crystalline by-products. The magnetic γ-Fe_2O_3/CMK-3 nanocomposite was formed by heating the as-prepared Fe_3O_4/CMK-3 composite at 150 °C for 2 h in air. The XRD patterns of both γ-Fe_2O_3/CMK-3 and Fe_3O_4/CMK-3 are almost the same (Fig. 3), matching both the maghemite γ-Fe_2O_3 (JCPDS card: 39-1346) and the magnetite Fe_3O_4 (JCPDS card: 19-0629), respectively. Both XRD patterns of magnetite and maghemite just differ in a few low intensity reflections (<5%) present at 2θ angle lower than 30°.[30] The low crystallinity of the maghemite γ-Fe_2O_3 resulted in the broad diffraction peaks, and thus it is more difficult to differentiate the maghemite and magnetite in CMK-3 based on their XRD patterns. Therefore, thermal analysis was further performed on both samples to unambiguously assign their crystal structures, discussed below (Fig. 4).

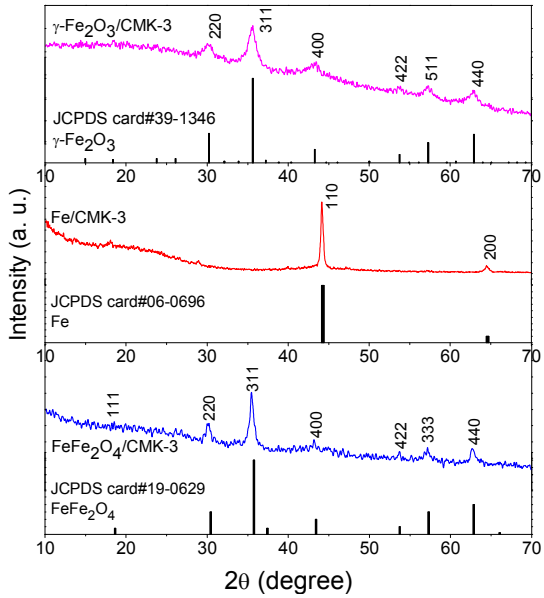

Fig. 3 Wide-angle XRD patterns of Fe_3O_4/CMK-3, Fe/CMK-3, and γ-Fe_2O_3/CMK-3 composites, and their corresponding JCPDS standard files for comparison.

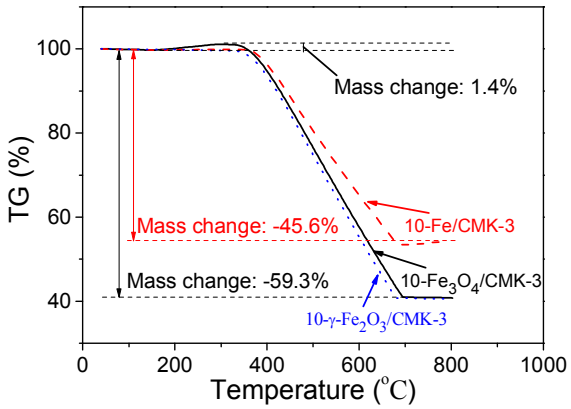

Fig. 4 TG curves of the 10-Fe_3O_4/CMK-3, 10-Fe/CMK-3, and 10-γ-Fe_2O_3/CMK-3 composite powders in air flow.

Fig. 4 shows the TG curves of 10-Fe_3O_4/CMK-3, 10-Fe/CMK-3 and 10-γ-Fe_2O_3/CMK-3 composites in air atmosphere. The heat-treatment of magnetic Fe-containing CMK-3 composites from room temperature to 800 °C in air will combust carbon as well as transform magnetic Fe-containing species to non-magnetic α-Fe_2O_3. Due to the combustion of carbon in the composite in the temperature range of 400-700 °C, 10-γ-Fe_2O_3/CMK-3 powder lost about 59.3% of total mass, which is close to the carbon content in the original composite (α-Fe_2O_3/CMK-3). Because γ-Fe_2O_3 gradually transformed into α-Fe_2O_3 without any mass change when increasing the temperature from room temperature to 380 °C,[31] the mass of 10-γ-Fe_2O_3/CMK-3 composite didn't change at the temperature lower than 380 °C in air. It should be noted that the weight of 10-Fe_3O_4/CMK-3 slightly increased at 200-380 °C, since Fe_3O_4 was oxidized to γ-Fe_2O_3 in air.[31] The maximum weight gain was 1.4 wt% at 300 °C, which is very close to the theoretical value 1.3 wt% for the oxidation of 10-Fe_3O_4/CMK-3 composite based on the content of Fe_3O_4 in air. Thus the TG data provide direct evidence for different crystal phases of magnetic species in 10-Fe_3O_4/CMK-3 and 10-γ-Fe_2O_3/CMK-3 nanocomposites. For 10-Fe/CMK-3 sample, the TG curve remained stable when the temperature was lower than 400 °C because of very slow oxidization of Fe nanoparticles. It is worth noting that the mass loss rate in the temperature range of 400-700 °C for 10-Fe/CMK-3 is evidently slower than those for both 10-Fe_3O_4/CMK-3 and 10-γ-Fe_2O_3/CMK-3, implying the gradual mass gain due to the oxidation of zero-valent Fe when the mass loss happened because of the carbon combustion. Thus the mass loss (45.6%) for 10-Fe/CMK-3 is evidently smaller than 59.3% for 10-γ-Fe_2O_3/CMK-3. TG showed that the pure CMK-3 started to lose mass at 450 °C,[15b] while the mass loss for the magnetic Fe-containing CMK-3 began at the lower temperature (380 °C), implying that the incorporation of Fe-containing species into the mesopores of CMK-3 can efficiently decrease the temperature of carbon oxidation. This finding is consistent with the previous report.[32]

Physical Chemistry Chemical Physics Accepted Manuscript

This journal is © The Royal Society of Chemistry 2012

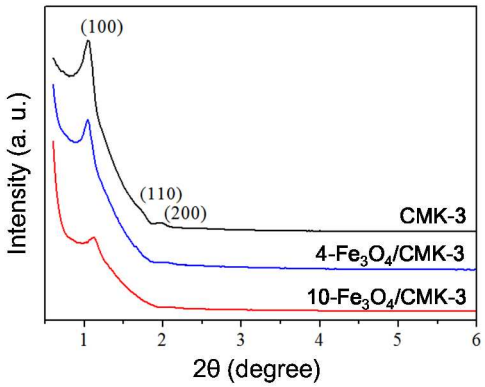

Fig. 5 Small-angle XRD patterns of CMK-3 and Fe_3O_4/CMK-3 composites.

After the reduction of α-Fe_2O_3/CMK-3 in 5% H_2/Ar, the resulting magnetic CMK-3 composites still maintain the ordered mesoporous structure. Taking the magnetic Fe_3O_4-filled CMK-3 composite as an example, the small-angle XRD pattern of 4-Fe_3O_4/CMK-3 is similar to that of the pristine CMK-3,[25] as shown in Fig. 5. One well-resolved diffraction peak around $2\theta = 1.04°$ with two weak peaks around $2\theta = 1.72°$ and 1.98° in the spectra belongs to a typical ordered mesoporous structure, corresponding to the hexagonal space group (*P6mm*) of (100), (110) and (200) diffraction peak. For 10-Fe_3O_4/CMK-3 with higher content of Fe_3O_4, the magnetic component occupies more mesopores and thus absorbs more X-ray energy. The X-ray diffraction path is also interfered and the contrast between the carbon skeleton and the mesopore is reduced, resulting in the broadening and widening of small-angle XRD peaks of magnetic mesoporous carbon composite. Furthermore, the diffraction peaks slightly shifts to high angle range for the magnetic mesoporous carbons, suggesting that the mesopore diameter decreases when magnetic nanoparticles are introduced into the mesopores of CMK-3.

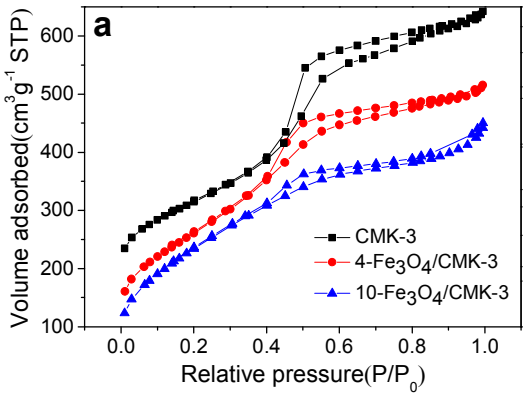

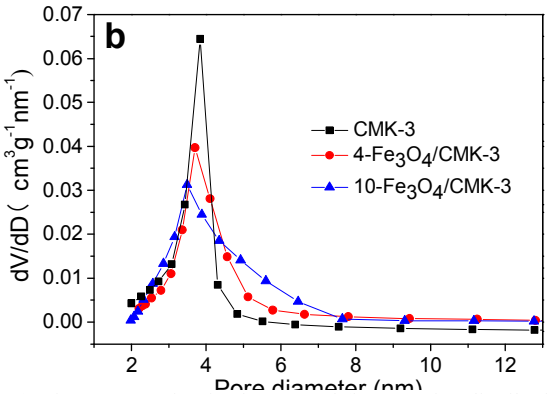

Fig. 6 (a) Nitrogen sorption isotherms and (b) pore size distributions of CMK-3 and Fe_3O_4/CMK-3 composites.

Because of the differences in the density of $Fe(NO_3)_3$ (1.68 g^{-1} cm^3) and ferrite (~ 5.2 g^{-1} cm^3), metallic Fe (7.86 g^{-1} cm^3), the *in situ* hydrolysis and pyrolysis processes resulted in a significant volume contraction of Fe-containing species. More than 70% volume in CMK-3 carbon occupied by $Fe(NO_3)_3$ precursor was released after *in situ* hydrolysis and pyrolysis and thus more pores in magnetic mesoporous carbons were generated. Fig. 6 shows the nitrogen sorption isotherms and pore size distributions of pure CMK-3 and Fe_3O_4/CMK-3 composites. It can be clearly observed that all nitrogen sorption isotherms are typical Langmuir Ⅳ curves with a H1 hysteresis loop, suggesting separate cylindrical elongate channels in the samples.[33] An obvious jump was occurred in the range of nitrogen relative pressure P/P_0 = 0.4-0.6, indicating uniform mesopore size distribution. The pore size distribution of the magnetic mesoporous carbons are mostly centered at 4 nm. The BET surface areas and pore volumes of the magnetic CMK-3 with a low iron loading (4-Fe_3O_4/CMK-3, 4-Fe/CMK-3 and 4-γ-Fe_2O_3/CMK-3) are as high as 943 m^2 g^{-1}, 1102 m^2 g^{-1}, 1081 m^2 g^{-1} and 0.78 cm^3 g^{-1}, 0.91 cm^3 g^{-1} and 0.82 cm^3 g^{-1}, respectively (Table 1). These values are lower than those (1319 m^2 g^{-1} and 1.35 cm^3 g^{-1}) of pure CMK-3, implying the pore filling by magnetic nanoparticles. Further decrease in those values is reasonably found for the composites with high iron content, but the BET surface areas are still high, 669 m^2 g^{-1}, 911 m^2 g^{-1}, and 873 m^2 g^{-1} for 10-Fe_3O_4/CMK-3, 10-Fe/CMK-3 and 10-γ-Fe_2O_3/CMK-3, respectively (Table 1). The high porosity in these magnetic samples would reduce the bulk density of the as-prepared magnetic CMK-3 powders undoubtedly, making it possible to design a light electromagnetic wave absorber.

Physical Chemistry Chemical Physics Accepted Manuscript

Table 1 Textural properties of CMK-3 and magnetic mesoporous carbon composites

Sample name	Filler content (wt.%)	BET area (m^2 g^{-1})	Pore volume (m^3 g^{-1})	Pore size (nm)
CMK-3	0	1329	1.35	4.2
4-Fe_3O_4/CMK-3	20.5	943	0.78	3.7
10-Fe_3O_4/CMK-3	39.2	669	0.47	3.4
4-Fe/CMK-3	15.7	1102	0.91	3.9
10-Fe/CMK-3	31.8	911	0.68	3.7
4-γ-Fe_2O_3/CMK-3	20.0	1081	0.82	4.1
10-γ-Fe_2O_3/CMK-3	40.0	873	0.64	3.8

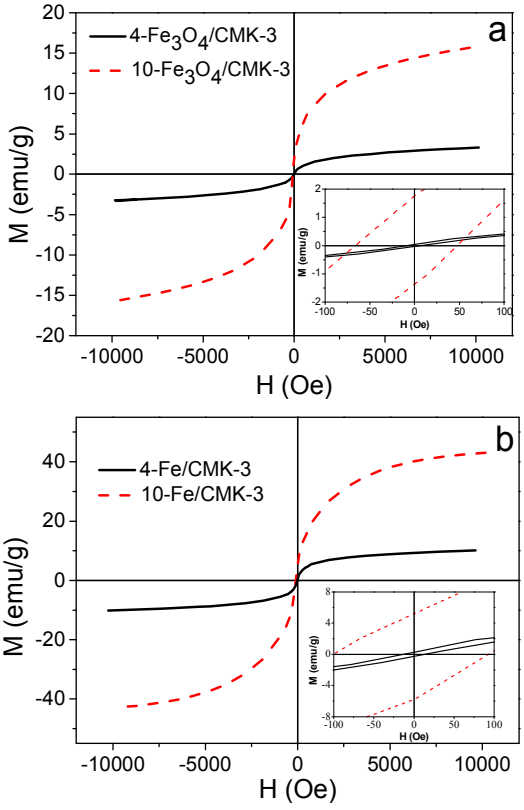

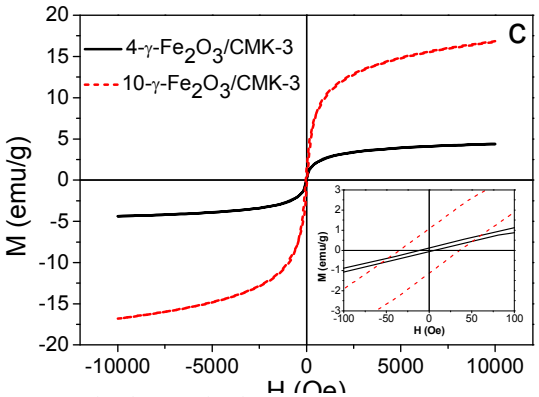

Fig. 7 Magnetic hysteresis loops at room temperature of (a) Fe_3O_4/CMK-3, (b) Fe/CMK-3 and (c) γ-Fe_2O_3/CMK-3. Insets in a-c are low field hysteresis curves.

Fe-based materials often have intriguing magnetic properties, and the structures, shape anisotropy and crystallinity of magnetic nanostructured materials can evidently influence their magnetic properties.[34] Thus, the magnetic properties of Fe_3O_4/CMK-3, Fe/CMK-3 and γ-Fe_2O_3/CMK-3 composites were further investigated. Fig. 7 show the magnetic hysteresis loops (M-H loops) combined with the expanded low-field hysteresis curves (insets) of the magnetic composites measured at room temperature, which indicate the magnetic properties including the saturation magnetization Ms and coercivity Hc, respectively. As shown Fig. 7a, the magnetic saturation is reached in the external field of about 10 kOe for Fe_3O_4/CMK-3. In general, Ms values of magnetic nanomaterials are lower than those of corresponding bulk materials because both the spin disorder on the surface and surface defects can significantly reduce the total magnetic moment.[35] Due to non-magnetism of carbon constituent and poor crystallinity of magnetic nanoparticles in the composite, the Ms value of 4-Fe_3O_4/CMK-3 is only 3.2 emu/g. Because of the nanoscale magnetic particles limited by the mesopore, thermal disturbance minimizes the coercive force of magnetic crystal. The inset in Fig. 7a clearly shows the Hc value is about 10 Oe for 4-Fe_3O_4/CMK-3. With the increase in the content of Fe, the Ms value of 10-Fe_3O_4/CMK-3 is 15.8 emu/g, still much lower than 92 emu/g for bulky Fe_3O_4.[29b] However the Hc value goes up to 66 Oe for 10-Fe_3O_4/CMK-3, implying the enhanced shape anisotropy of the magnetic crystals. Moreover, in the case of Fe/CMK-3 and γ-Fe_2O_3/CMK-3 composites, the Ms values are about 10.1 emu/g for 4-Fe/CMK-3 and 42.9 emu/g for 10-Fe/CMK-3, respectively, and the Hc values are about 15 Oe for 4-Fe/CMK-3 and 100 Oe for 10-Fe/CMK-3 (Figure 7b and the inset). The Ms values are about 4.4 emu/g for 4-γ-Fe_2O_3/CMK-3 and 15.8 emu/g for 10-γ-Fe_2O_3/CMK-3, respectively, and the Hc values are about 11 Oe for 4-γ-Fe_2O_3/CMK-3 and 36 Oe for 10-γ-Fe_2O_3/CMK-3, respectively (Fig. 7c and the inset). The Ms values for Fe/CMK-3 and γ-Fe_2O_3/CMK-3 composite are also significantly lower than the values of bulk materials (Ms_{Fe} = 217.6 emu/g; $Ms_{\gamma\text{-}Fe2O3}$ = 76 emu/g), respectively. It can be found that the Ms and Hc values for Fe/CMK-3, Fe_3O_4/CMK-3, and γ-Fe_2O_3/CMK-3 decreased as the following order: Ms_{Fe} >

Physical Chemistry Chemical Physics Accepted Manuscript

This journal is © The Royal Society of Chemistry 2012

$Ms_{Fe3O4} \approx Ms_{\gamma\text{-}Fe2O3}$; $Hc_{Fe} > Hc_{Fe3O4} > Hc_{\gamma\text{-}Fe2O3}$. This order is a key factor to determine their ability of absorbing microwave.

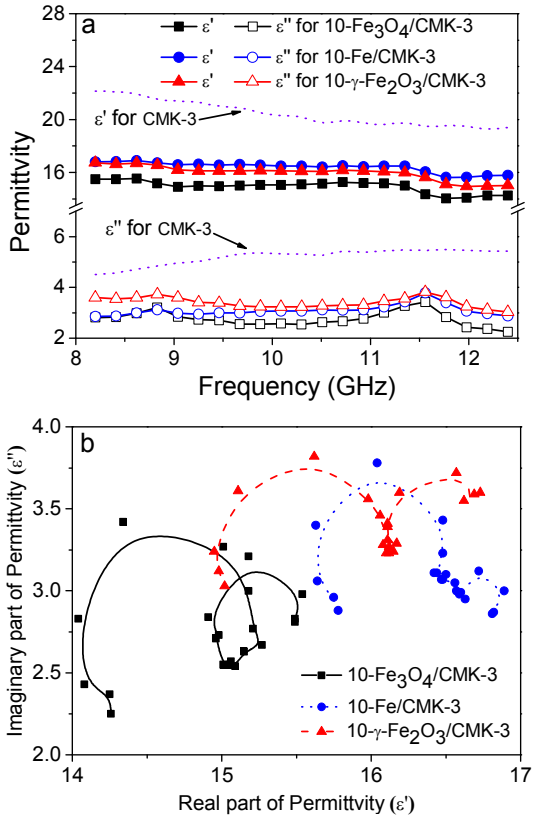

Fig. 8 (a) Frequency dependences of complex permittivity and (b) typical Cole-Cole semicircles for 10-Fe_3O_4/CMK-3, 10-Fe/CMK-3 and 10-γ-Fe_2O_3/CMK-3 composites

In order to study the interaction mechanism of magnetic mesoporous carbons and microwave, the complex permittivity of these magnetic mesoporous carbons were measured in the range of *X*-band. Fig. 8a and S2 shows the frequency dependent complex permittivity of pure CMK-3 and magnetic mesoporous carbons that are mixed with resin (resin content: 80 wt%). Because of its good conductivity, carbon has high complex permittivity. Therefore, when carbon is composited with Fe_3O_4, Fe, or γ-Fe_2O_3, the complex permittivity of the as-formed composite decreases compared to that of pure carbon (Fig. 8a). The trends of permittivity with frequency for the magnetic composites are similar to that for pure CMK-3, but the permittivity values of the magnetic composites are evidently higher. The real part of complex permittivity (ε') of 4-Fe_3O_4/CMK-3 composite decreases from 19.1 to 15.8 (average: 17.1) with increasing the frequency in the *X*-band (Fig. S2), while the imaginary part (ε'') fluctuates in the range of 2.3-4.1 (average: 3.1). When more magnetic nanoparticles are confined within the mesopore of CMK-3 carbon, the complex permittivity of the composites evidently decreases (Fig. S2). For magnetic composites with higher contents of Fe-containing species, the ε' and ε'' values for three magnetic composites are almost independent of magnetic species, but a little change can be found in the following order: ε' (10-Fe/CMK-3) > ε' (10-γ-Fe_2O_3/CMK-3) > ε' (10-Fe_3O_4/CMK-3); ε'' (10-γ-Fe_2O_3/CMK-3) > ε'' (10-Fe/CMK-3) > ε'' (10-Fe_3O_4/CMK-3) (Fig. 8a). Fig. 8b presents the curve characteristic of ε' versus ε''. Three magnetic composites all show a clear segment of two distorted Cole-Cole semicircles, suggesting the existence of multiple dielectric relaxations in the magnetic nanocomposites. They are consistent with the change of their complex permittivity. The resulting multiple relaxations can result from the interface polarization which are caused by the heterogeneous interfaces of magnetic nanoparticles and CMK-3 carbon, and CMK-3 carbon and resin matrix because magnetic mesoporous carbon composites have very high specific surface areas (600-1100 m^2 g^{-1}).[36]

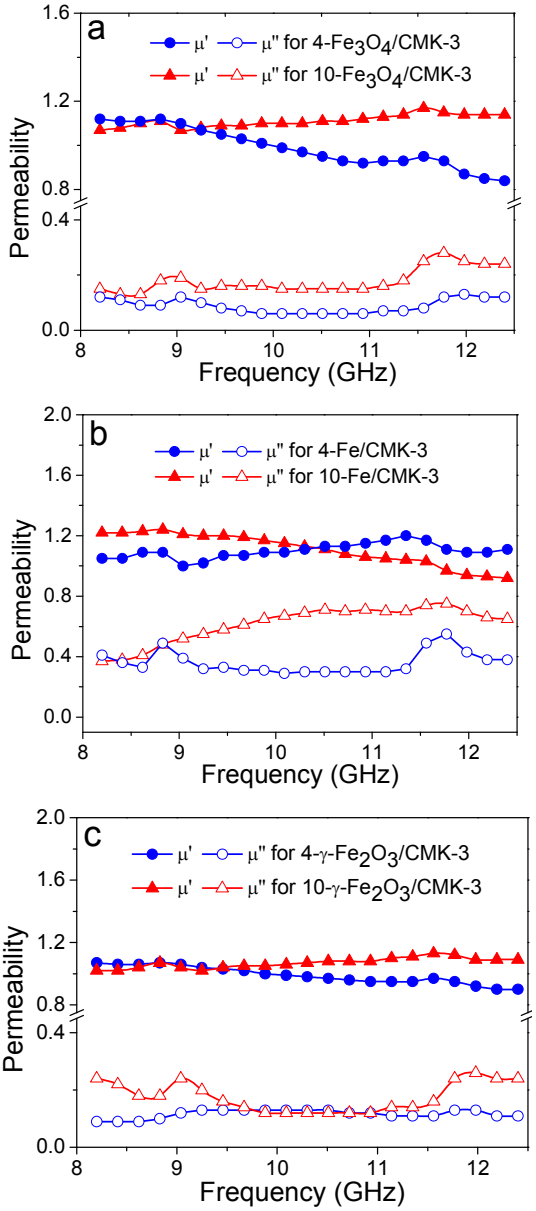

Fig. 9 Frequency dependence of complex permeability for (a) Fe_3O_4/CMK-3, (b) Fe/CMK-3 and (c) γ-Fe_2O_3/CMK-3.

Fig. 9 displays the frequency dependence of complex permeability of magnetic mesoporous carbons mixed with resin. The real part of complex permeability (μ') of 4-Fe_3O_4/CMK-3

Physical Chemistry Chemical Physics Accepted Manuscript

sample decreases from 1.1 to 0.8 in the *X*-band, while its imaginary part of complex permeability (μ'') retains at 0.06-0.12 (Fig. S3). For the sample with higher content of Fe_3O_4, the complex permeability of 10-Fe_3O_4/CMK-3 significantly increases: μ' is about 1.1, and μ'' increases to about 0.2 (Fig. 9a). When the magnetic species are Fe nanoparticles, the μ'' values of Fe/CMK-3 dramatically increase due to higher Ms and Hc of Fe as mentioned above. The μ'' values for 4-Fe/CMK-3 and 10-Fe/CMK-3 are as high as 0.4 and 0.8, respectively (Fig. 9b), which are significantly higher than those for Fe_3O_4/CMK-3 samples. Due to the lower magnetism of γ-Fe_2O_3 than Fe, the μ'' values of γ-Fe_2O_3/CMK-3 samples are smaller than those of Fe/CMK-3, and comparable to those of Fe_3O_4/CMK-3 (Fig. 9).

As seen in Fig. 9, two weak resonance peaks are observed at 9 and 12 GHz, respectively, implying that there are strong magnetic loss resonances at these two frequencies for magnetic mesoporous carbons. The magnetic losses for magnetic materials such as ferrite are mainly derived from domain wall resonance, hysteresis loss, eddy current loss, natural resonance, *etc*.[37] The domain wall resonance normally happens at the frequency lower than 100 MHz, and thus it can be neglected in the microwave range. The hysteresis loss is produced in a very strong external magnetic field, and there is no hysteresis loss in weak magnetic field derived from microwave. Therefore the eddy current loss and natural resonance loss are key factors affecting magnetic loss in the frequency range of microwave.

The confinement of the magnetic constituents within mesoporous carbons evidently increases the μ'' values of the magnetic nanocomposites compared to that of pure CMK-3 carbon (Fig. 9 and S3). Thus, the magnetic loss in the electromagnetic field will enhance the ability of absorbing microwave for the composite. Because Fe_3O_4, Fe, and γ-Fe_2O_3 within the mesopore of CMK-3 are ferro-magnetic, circulating induced current, named as eddy current, is formed inside the magnetic nanoparticles when the magnetic nanocomposite exists in an alternating electromagnetic field. The eddy-current generating heat energy inside the ferro-magnetic particles is a process of energy loss, also called as eddy-current loss. According to the literatures,[37a, 38] there is a relationship in the eddy-current loss as following equation:

$$f^{-1}(\mu')^{-2}\mu'' \approx \frac{2\pi\mu_0\sigma d^2}{3}$$

where f is the frequency of microwave, μ_0 is the permeability of vacuum, σ is the electric conductivity of microwave absorber, and d is the particle diameter of microwave absorber. If the magnetic loss just results from eddy-current loss, the value of $f^{-1}(\mu')^{-2}\mu''$ should be constant.[37a, 38] Fig. 10 shows the values of $f^{-1}(\mu')^{-2}\mu''$ as a function of frequency for 10-Fe_3O_4/CMK-3, 10-Fe/CMK-3 and 10-γ-Fe_2O_3/CMK-3 composites. It can be found that the $f^{-1}(\mu')^{-2}\mu''$ value of 10-Fe/CMK-3 significantly changes as the frequency increases, implying that its magnetic loss contains not only eddy-current loss, but also magnetic resonance loss, *etc*. Both $f^{-1}(\mu')^{-2}\mu''$ values of 10-γ-Fe_2O_3/CMK-3 and 10-Fe_3O_4/CMK-3 are nearly independent of the frequency, showing that their magnetic losses are mainly ascribed to eddy-current loss.

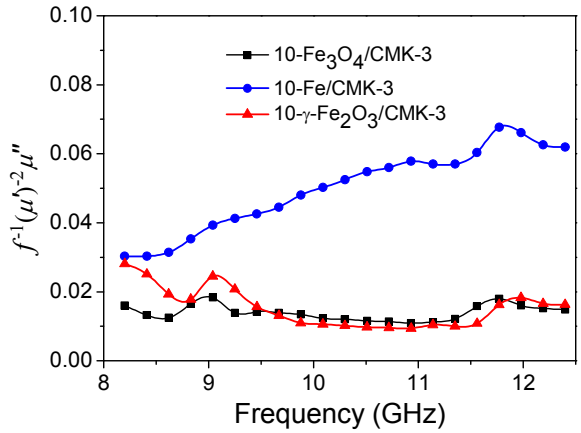

Fig. 10 Values of $f^{-1}(\mu')^{-2}\mu''$ as a function of frequency for 10-Fe_3O_4/CMK-3, 10-Fe/CMK-3 and 10-γ-Fe_2O_3/CMK-3 composites

In natural resonance, the resonance frequency f_r and anisotropy field H_a are related as following: $2\pi f_r = \gamma H_a$ (γ is the gyromagnetic ratio). And H_a is proportional to the anisotropy constant K_1 of magnetic crystal, written as $H_a = 4 \mid K_1 \mid /3\mu_0 Ms$.[39] The anisotropy constant K_1 of the cubic Fe_3O_4, Fe, and γ-Fe_2O_3 is -1.1×10^4, 4.8×10^4, -2.5×10^4 J/m^3, respectively. Therefore, the intrinsic resonance frequency f_r in bulk magnetic material is almost several hundreds of Hz. However, for nanosized magnetic particles, H_a on the surface of magnetic particles is strongly influenced by nanometer size effect, and it greatly increases accordingly. It will possibly result in the resonance frequency f_r existed in the range of GHz.[40] Thus, the magnetic loss of Fe/CMK-3 nanocomposite in the *X*-band is partly due to natural resonance loss derived from nanosized magnetic nanoparticles.

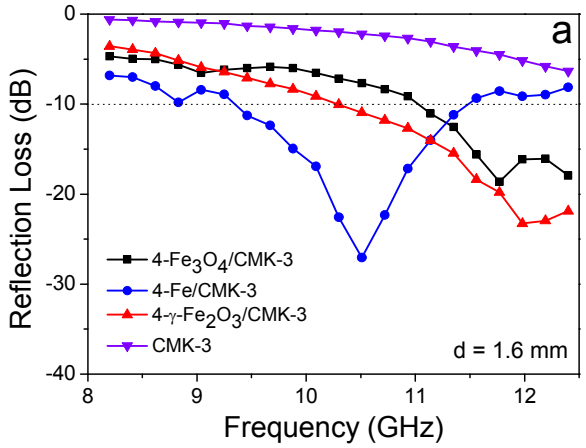

Physical Chemistry Chemical Physics Accepted Manuscript

This journal is © The Royal Society of Chemistry 2012

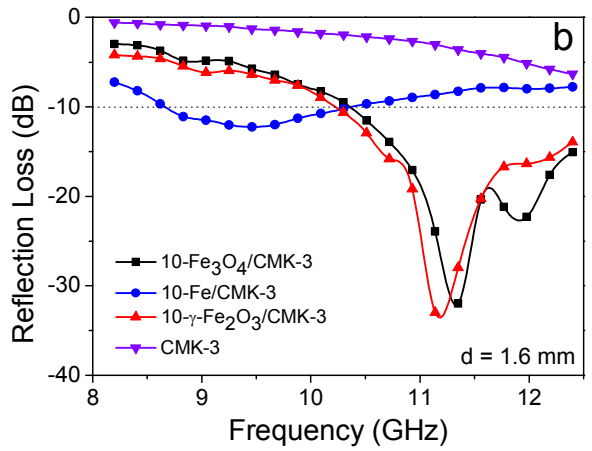

Fig. 11 Frequency dependence of the RL values of the (a) 4-Fe_3O_4/CMK-3, 4-Fe/CMK-3, 4-γ-Fe_2O_3/CMK-3 and (b) 10-Fe_3O_4/CMK-3, 10-Fe/CMK-3, 10-γ-Fe_2O_3/CMK-3 composite samples with a matching thickness of 1.6 mm

According to the transmission line theory for a single-layer absorber, the measured values of ε', ε'', μ', and μ'' are used to determine the RL values of the as-prepared composites based on a model for a single-layer plane-wave absorber.[41] Fig. 11 displays the calculated RL over the *X*-band of Fe_3O_4/CMK-3, Fe/CMK-3, and γ-Fe_2O_3/CMK-3 samples, where the maximum RL is equivalent to the maximum absorption of incident microwave power. It can be found that all magnetic mesoporous carbons demonstrate much better microwave absorbing properties than pure CMK-3. As a function of frequency in a matching thickness of 1.6 mm, 4-Fe_3O_4/CMK-3, 4-Fe/CMK-3, and 4-γ-Fe_2O_3/CMK-3 sample show a maximum RL of -18.6 dB at 11.8 GHz, -27 dB at10.5 GHz, and -23 dB at 12 GHz, respectively. With increasing the contents of Fe_3O_4 and γ-Fe_2O_3 in CMK-3, both 10-Fe_3O_4/CMK-3 and 10-γ-Fe_2O_3/CMK-3 samples have a maximum RL of up to -32 dB. The effective absorption bandwidth with a RL below -10 dB for these two samples ranges from 10.3 to 12.4 GHz (2.1 GHz in width). The present magnetic mesoporous carbon nanocomposites have better microwave absorption properties than other previously reported nanocomposites as microwave absorbers. For example, the ternary Fe_3O_4@polyaniline-based polymers only exhibited microwave-absorbing properties with a maximum RL about -18 dB.[42] The porous Fe_3O_4/Fe/SiO_2 core/shell nanorods had a medium RL of -17 dB.[22a] *In situ* polymerized and grafted CMK-3@PMMA composite had a RL value of -27 dB.[18] It can be considered that the introduction of magnetic constituents into CMK-3 mesoporous carbon improves the magnetic loss and impedance matching performance of mesoporous carbon and reduces the reflection of microwave at the interface between air and absorber. At the same time, the magnetic nanoparticles increase the interface relaxation and scatter the incident microwave, and thus promote the ability of absorbing microwave. So the performance of absorbing microwave for magnetic mesoporous carbon nanocomposites is greatly improved. The higher contents of the magnetic nanoparticles the better ability of absorbing microwave for the composites. At the same time, ordered carbon mesostructures of magnetic composite can effectively improve the absorption by multi-absorption from intra-re-reflecting and scattering the incident microwave in the confined space and at the interface.[16-17] However, 4-Fe/CMK-3 has a maximum RL of -27 dB while it is just -12 dB for 10-Fe/CMK-3 with higher content of Fe. Fe is highly electrically conductive and itself can reflect much electromagnetic wave. The high content of Fe in the composite weakens the impedance matching effect from the addition of magnetic Fe particles. Therefore, the composite with suitable amount of Fe nanoparticles has excellent absorbing microwave performance.

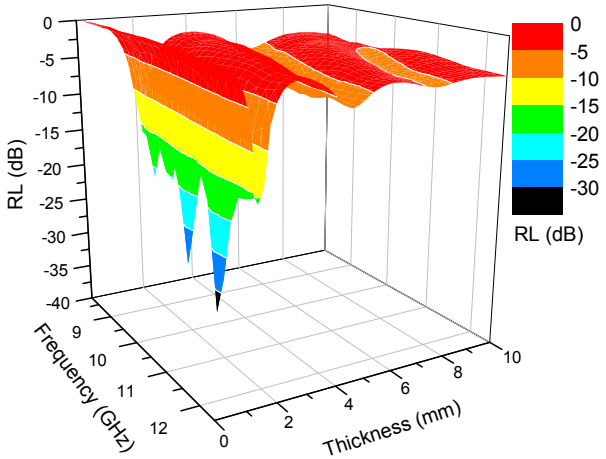

Fig. 12 The RL value of 10-Fe_3O_4/CMK-3 as a function of thickness and frequency.

Fig. 12 shows the RL values of the 10-Fe_3O_4/CMK-3 composite at as a function of thickness over the *X*-band. The composite has a strong absorbing band with RL values < -10 dB at the matching thickness of 1.6-2.0 mm. The maximum RL value is -32 dB, and the effective absorption bandwidth is over 2 GHz. With increasing the matching thickness, the absorbing band gradually shifts to the range of low frequency. Therefore, the Fe_3O_4 or γ-Fe_2O_3 filled mesoporous carbons with low thickness has good ability of absorbing microwave, and they are a kind of high-performance microwave absorber.

4. Conclusions

The magnetic mesoporous carbon composites were successfully prepared by filling the mesopores with $Fe(NO_3)_3$, followed by *in situ* hydrolysis, pyrolysis, and reduction process. The magnetic nanocomposites have high contents of magnetic constituents, but the magnetic nanoparticles are homogeneously incorporated into the pores of mesoporous carbon, confirmed by the electron microscopy measurements. The as-prepared magnetic mesoporous carbon composites still retain highly ordered mesoporous structure determined by small-angle XRD, but they also have high specific surface areas (600-1100 $m^2 g^{-1}$) and pore volumes obtained from nitrogen sorption measurements at -196 °C. By measuring the magnetic hysteresis loops of these magnetic nanocomposites, it is found that the magnetic constituents are poorly-crystalline nanoparticles. Their saturation magnetization Ms is evidently

Physical Chemistry Chemical Physics Accepted Manuscript

smaller than bulky magnetic materials, and the thermal disturbance minimizes the coercive force of magnetic crystal.

When introducing magnetic Fe_3O_4, Fe, and γ-Fe_2O_3 nanoparticles into mesoporous carbons, the complex permittivity decreases while the complex permeability increases compared to pure mesoporous carbon. Thus the impedance matching performance of these composites is improved, which increases the microwave absorbing ability. The magnetic constituents in the nanocomposites greatly increase magnetic loss ability, and high specific surface areas are beneficial for interface polarization. The specific ordered mesochannels of magnetic composites lead to multi-reflection and multi-scattering of the incident microwave. As a result, 10-Fe_3O_4/CMK-3 and 10-γ-Fe_2O_3/CMK-3 composites exhibit excellent microwave absorption properties. The maximum RL is -32 dB for the composite with a matching thickness of 1.6 mm and the bandwidth (RL lower than -10 dB) is over 2 GHz in the *X*-band. The present results show that the as-prepared magnetic mesoporous carbon nanocomposites can be used as highly effective microwave absorbing materials, and their ability of absorbing microwave can be adjusted by introducing different magnetic components and controlling the contents of magnetic nanoparticles. This research opens a new method and idea for developing novel mesoporous carbon composites as high-performance microwave absorbing materials.

Acknowledgements

The authors thank the Youth Innovation Fund (Grant No. Y21ZC8180G) from Shanghai Institute of Ceramics, the One Hundred Talent Plan of Chinese Academy of Sciences, National Natural Science Foundation of China (Grant No. 21307145) for the financial support.

Notes and references

[a] *State Key Laboratory of High Performance Ceramics and Superfine Microstructure, Shanghai Institute of Ceramics, Chinese Academy of Science, Shanghai 200050, P. R. China. Email: Jiacheng.wang@mail.sic.ac.cn; qianliu@sunm.shcnc.ac.cn; Tel: 0086-21-52412612. Fax: 0086-21-52413122*
[b] *University of Chinese Academy of Sciences, Beijing 100049, P. R. China.*
Electronic Supplementary Information (ESI) available: Additional figures mentioned in the text. See DOI: 10.1039/b000000x/

1. a) R. Redl, P. Tenti and J. Daan van Wyk, *Spectrum, IEEE*, 1997, **34**, 32; b) S. Geetha, K. Satheesh Kumar, C. R. Rao, M. Vijayan and D. Trivedi, *J. Appl. Polym. Sci.*, 2009, **112**, 2073.
2. J. Liu, J. Tang and J. J. Gooding, *J. Mater. Chem.*, 2012, **22**, 12435.
3. a) D. R. Dreyer, H.-P. Jia and C. W. Bielawski, *Angew. Chem.*, 2010, **122**, 6965; b) D. R. Dreyer and C. W. Bielawski, *Chem. Sci.*, 2011, **2**, 1233; c) L.-P. Guo, J. Bai, H.-O. Liang, C.-P. Li, W.-Y. Sun and Q.-R. Meng, *J. Inorg. Mater.*, 2014, **29**, 814.
4. a) R. Liu, D. Wu, X. Feng and K. Müllen, *Angew. Chem.*, 2010, **122**, 2619; b) Y. Li, W. Zhou, H. Wang, L. Xie, Y. Liang, F. Wei, J.-C. Idrobo, S. J. Pennycook and H. Dai, *Nat. Nanotech.*, 2012, **7**, 394.
5. a) J. Wang, A. Heerwig, M. R. Lohe, M. Oschatz, L. Borchardt and S. Kaskel, *J. Mater. Chem.*, 2012, **22**, 13911; b) J. Wang, I. Senkovska, S. Kaskel and Q. Liu, *Carbon*, 2014, **75**, 372; c) J. Wei, D. Zhou, Z. Sun, Y. Deng, Y. Xia and D. Zhao, *Adv. Funct. Mater.*, 2013, **23**, 2322; d) J. Wang, M. Oschatz, T. Biemelt, L. Borchardt, I. Senkovska, M. R. Lohe and S. Kaskel, *J. Mater. Chem.*, 2012, **22**, 23893; e) J. Wang, I. Senkovska, M. Oschatz, M. R. Lohe, L. Borchardt, A. Heerwig, Q. Liu and S. Kaskel, *J. Mater. Chem. A*, 2013, **1**, 10951; f) J. Wang, I. Senkovska, M. Oschatz, M. R. Lohe, L. Borchardt, A. Heerwig, Q. Liu and S. Kaskel, *ACS Appl. Mater. Interfaces*, 2013, **5**, 3160.
6. a) E. Frackowiak, *Phys. Chem. Chem. Phys.*, 2007, **9**, 1774; b) J. Wang and S. Kaskel, *J. Mater. Chem.*, 2012, **22**, 23710; c) M.-G. Deng, R.-Q. Wang and Y.-H. Feng, *J. Inorg. Mater.*, 2014, **29**, 245; d) L.-H. Sun, H.-B. Liu, X.-H. Xia and Y.-D. He, *J. Inorg. Mater.*, 2013, **28**, 267.
7. a) M. Teng, J. Qiao, F. Li and P. K. Bera, *Carbon*, 2012, **50**, 2877; b) A. Vinu, K. Z. Hossian, P. Srinivasu, M. Miyahara, S. Anandan, N. Gokulakrishnan, T. Mori, K. Ariga and V. V. Balasubramanian, *J. Mater. Chem.*, 2007, **17**, 1819; c) G. P. Mane, S. N. Talapaneni, C. Anand, S. Varghese, H. Iwai, Q. Ji, K. Ariga, T. Mori and A. Vinu, *Adv. Funct. Mater.*, 2012, **22**, 3596; d) L.-Q. Duan, Q.-S. Ma and Z.-H. Chen, *J. Inorg. Mater.*, 2013, **28**, 1051.
8. a) M. H. Al-Saleh, W. H. Sadaah and U. Sundararaj, *Carbon*, 2013, **60**, 146; b) J.-H. Oh, K.-S. Oh, C.-G. Kim and C.-S. Hong, *Compos. Part B-ENG.*, 2004, **35**, 49.
9. a) M.-S. Cao, W.-L. Song, Z.-L. Hou, B. Wen and J. Yuan, *Carbon*, 2010, **48**, 788; b) N. Zhao, T. Zou, C. Shi, J. Li and W. Guo, *Mater. Sci. Eng. B*, 2006, **127**, 207; c) X. Luo and D. Chung, *Compos. Part B-ENG.*, 1999, **30**, 227; d) Y. Yang, M. C. Gupta, K. L. Dudley and R. W. Lawrence, *Adv. Mater.*, 2005, **17**, 1999.
10. a) M. H. Al-Saleh and U. Sundararaj, *Carbon*, 2009, **47**, 1738; b) N. Li, Y. Huang, F. Du, X. He, X. Lin, H. Gao, Y. Ma, F. Li, Y. Chen and P. C. Eklund, *Nano Lett.*, 2006, **6**, 1141; c) T. K. Gupta, B. P. Singh, S. R. Dhakate, V. Singh and R. B. Mathur, *J. Mater. Chem. A*, 2013, **1**, 9138; d) M.-S. Cao, J. Yang, W.-L. Song, D.-Q. Zhang, B. Wen, H.-B. Jin, Z.-L. Hou and J. Yuan, *ACS Appl. Mater. Interfaces*, 2012, **4**, 6949; e) C. S. Xiang, Y. B. Pan, X. J. Liu, X. W. Sun, X. M. Shi and J. K. Guo, *App. Phys. Lett.*, 2005, **87**, 123103.
11. R. Kumar, S. R. Dhakate, P. Saini and R. B. Mathur, *RSC Adv.*, 2013, **3**, 4145.
12. a) H.-B. Zhang, Q. Yan, W.-G. Zheng, Z. He and Z.-Z. Yu, *ACS Appl. Mater. Interfaces*, 2011, **3**, 918; b) Z. Chen, C. Xu, C. Ma, W. Ren and H. M. Cheng, *Adv. Mater.*, 2013, **25**, 1296; c) V. K. Singh, A. Shukla, M. K. Patra, L. Saini, R. K. Jani, S. R. Vadera and N. Kumar, *Carbon*, 2012, **50**, 2202.
13. a) R. Ryoo, S. H. Joo, M. Kruk and M. Jaroniec, *Adv. Mater.*, 2001, **13**, 677; b) S. Jun, S. H. Joo, R. Ryoo, M. Kruk, M. Jaroniec, Z. Liu, T. Ohsuna and O. Terasaki, *J. Am. Chem. Soc.*, 2000, **122**, 10712.
14. C. Liang, Z. Li and S. Dai, *Angew. Chem. Int. Ed.*, 2008, **47**, 3696.
15. a) J. Lee, J. Kim and T. Hyeon, *Adv. Mater.*, 2006, **18**, 2073; b) J. Wang and Q. Liu, *J. Phys. Chem. C*, 2007, **111**, 7266.
16. J. C. Wang, C. S. Xiang, Q. Liu, Y. B. Pan and J. K. Guo, *Adv. Funct. Mater.*, 2008, **18**, 2995.
17. J. Wang, H. Zhou, J. Zhuang and Q. Liu, *Sci. Rep.*, 2013, **3**, 3252.
18. H. Zhou, J. Wang, J. Zhuang and Q. Liu, *Nanoscale*, 2013, **5**, 12502.
19. H. Zhou, J. Wang, J. Zhuang and Q. Liu, *RSC Adv.*, 2013, **3**, 23715.

Physical Chemistry Chemical Physics Accepted Manuscript

 This journal is © The Royal Society of Chemistry 2012

20. a) J. Li, H.-B. Liu and L. Yang, *J. Inorg. Mater.*, 2014, **29**, 470; b) X.-Y. Wu, S.-M. Li, J.-H. Liu, M. Yu and B. Wang, *J. Inorg. Mater.*, 2014, **29**, 845.
21. Q. Liu, D. Zhang and T. Fan, *App. Phys. Lett.*, 2008, **93**, 013110.
22. a) Y. Chen, P. Gao, C. Zhu, R. Wang, L. Wang, M. Cao and X. Fang, *J. Appl. Phys.*, 2009, **106**, 054303; b) H. Lin, H. Zhu, H. Guo and L. Yu, *Mater. Res. Bull.*, 2008, **43**, 2697.
23. Z. Wu, W. Li, P. A. Webley and D. Zhao, *Adv. Mater.*, 2012, **24**, 485.
24. a) Z. Wu, Q. Li, D. Feng, P. A. Webley and D. Zhao, *J. Am. Chem. Soc.*, 2010, **132**, 12042; b) Z. Gu, B. Deng and J. Yang, *Microporous Mesoporous Mater.*, 2007, **102**, 265; c) A.-H. Lu, J.-J. Nitz, M. Comotti, C. Weidenthaler, K. Schlichte, C. W. Lehmann, O. Terasaki and F. Schuth, *J. Am. Chem. Soc.*, 2010, **132**, 14152; d) Y. Zhai, Y. Dou, X. Liu, B. Tu and D. Zhao, *J. Mater. Chem.*, 2009, **19**, 3292.
25. A. H. Lu, W. Schmidt, A. Taguchi, B. Spliethoff, B. Tesche and F. Schuth, *Angew. Chem. Int. Ed.*, 2002, **41**, 3489.
26. S. Brunauer, P. H. Emmett and E. Teller, *J. Am. Chem. Soc.*, 1938, **60**, 309.
27. a) J. Wang, X. Yu, Y. Li and Q. Liu, *J. Phys. Chem. C*, 2007, **111**, 18073; b) J. Wang and Q. Liu, *J. Mater. Res.*, 2005, **20**, 2296.
28. Y. L. Chueh, M. W. Lai, J. Q. Liang, L. J. Chou and Z. L. Wang, *Adv. Funct. Mater.*, 2006, **16**, 2243.
29. a) H. H. P. Yiu, M. A. Keane, Z. A. D. Lethbridge, M. R. Lees, A. J. El Haj and J. Dobson, *Nanotechnology*, 2008, **19**; b) G. Sun, B. Dong, M. Cao, B. Wei and C. Hu, *Chem. Mater.*, 2011, **23**, 1587.
30. F. Jiao, J.-C. Jumas, M. Womes, A. V. Chadwick, A. Harrison and P. G. Bruce, *J. Am. Chem. Soc.*, 2006, **128**, 12905.
31. R. M. Cornell and U. Schwertmann, *The iron oxides: structure, properties, reactions, occurrences and uses*, John Wiley & Sons, 2006.
32. L. M. Xiong, E. H. Sekiya, S. Wada and K. Saito, *ACS Appl. Mater. Interfaces*, 2009, **1**, 2509.
33. K. S. Sing, *Adv. Colloid Interface Sci.*, 1998, **76**, 3.
34. J.-H. Lim, W.-S. Chae, H.-O. Lee, L. Malkinski, S.-G. Min, J. Wiley, J.-H. Jun, S.-H. Lee and J.-S. Jung, *J. Appl. Phys.*, 2010, **107**, 09A334.
35. M. McHenry and D. Laughlin, *Acta Mater.*, 2000, **48**, 223.
36. a) P. C. Watts, W. K. Hsu, A. Barnes and B. Chambers, *Adv. Mater.*, 2003, **15**, 600; b) X. Zhang, X. Dong, H. Huang, D. Wang, B. Lv and J. Lei, *Nanotechnology*, 2007, **18**, 275701.
37. a) X. Zhang, X. Dong, H. Huang, Y. Liu, W. Wang, X. Zhu, B. Lv, J. Lei and C. Lee, *App. Phys. Lett.*, 2006, **89**, 053115; b) V. Petrov and V. Gagulin, *Inorg. Mater.*, 2001, **37**, 93.
38. M. Wu, Y. Zhang, S. Hui, T. Xiao, S. Ge, W. Hines, J. Budnick and G. Taylor, *App. Phys. Lett.*, 2002, **80**, 4404.
39. B. D. Cullity and C. D. Graham, *Introduction to magnetic materials*, John Wiley & Sons, 2011.
40. H. Wu, L. Wang, Y. Wang, S. Guo and Z. Shen, *J. Alloy. Comp.*, 2012, **525**, 82.
41. D. Micheli, R. Pastore, C. Apollo, M. Marchetti, G. Gradoni, V. M. Primiani and F. Moglie, *Microwave Theory and Techniques, IEEE Transactions on*, 2011, **59**, 2633.
42. W. Wei, X. Yue, Y. Zhou, Y. Wang, Z. Chen, M. Zhu, J. Fang and Z. Jiang, *RSC Adv.*, 2014, **4**, 11159.

Physical Chemistry Chemical Physics Accepted Manuscript